Modification of directed-loop algorithm for continuous space simulation of bosonic systems

Yasuyuki Kato, Takafumi Suzuki, and Naoki Kawashima
Institute for Solid State Physics, University of Tokyo, 5-1-5 Kashiwa-no-ha, Kashiwa, Chiba 277-8581, Japan
(Received 7 March 2007; published 14 June 2007)

We modify the directed-loop algorithm (DLA) to solve the problem that typically arises from large on-site interaction. The large on-site interaction is inevitable when one tries to simulate a Bose gas system in continuum by discretizing the space with small lattice spacings. While the efficiency of a straightforward application of DLA decreases as the mesh becomes finer, the performance of the new method does not depend on it except for the trivial factor due to the increase in the number of lattice points.

DOI: 10.1103/PhysRevE.75.066703 PACS number(s): 02.70.Ss, 03.75.Hh, 02.70.Tt

I. INTRODUCTION

Bose-Einstein condensation (BEC) in atomic gases trapped in an external potential was observed in a laboratory in 1995 [1]. Since then, the bosonic systems have been studied extensively. A recent focus of attention is the quantum phase transition from a superfluid to a Mott insulator in a gas of ultracold atoms [2]. The experiment was carried out in a three-dimensional optical lattice potential. The atoms move freely all over the lattice in the superfluid phase. The transition occurs as the depth of the lattice potential is increased. After the transition, each atom is localized at an individual lattice site. Another topic of current interest is the observation of the supersolid phase in the solid ^{4}He [3]. Kim and Chan observed an anomaly in the rotational inertia at the critical temperature. Several theoretical investigations were carried out, such as Monte Carlo simulations of Bose systems on a two-dimensional triangular lattice [4–7] and in a continuous space [8].

The Monte Carlo sampling of world-line configurations based on the Feynman path integral is one of the most efficient presently-known method to deal with such bosonic systems. There are a few variants of the method designed for continuous bosonic systems that we discuss in the present paper. In their pioneering work, Ceperley and Pollock [9,10] approximated world lines by jagged lines in continuous real space and discrete imaginary time. An update cycle of world-line configurations is executed in two steps, the first step with the "bisection method" and second with the "permutation sampling method." Using these methods, they simulated the superfluid transition in a system of $N=64$ ^{4}He atoms in three dimensions. Quantities such as energy and diagonal correlations were successfully calculated.

However, in order to calculate off-diagonal quantities such as the superfluid fraction ρ_S accurately, we must consider larger number of atoms. Recently, to solve this problem, Boninsegni *et al.* [11] generalized the worm algorithm, which is originally developed for lattice systems and has capability to treat a large number of degrees of freedom, to the continuous cases. In their method, the world lines are treated as jagged lines as in the method of Ceperley *et al.* However, updates of world-line configurations are achieved by using a worm that consists of a pair of discontinuity points. One of the discontinuity points, hereafter referred to as the *head*, moves stochastically in the space-time and changes the local state on the way. To be more specific, an update cycle is a combination of four sets of processes called "open/close," "insert/remove," "advance/recede," and "swap." The "open" and "insert" operations create a worm whereas the "close" and "remove" operations annihilate it. The "advance/recede" operation slides the head along the vertical (i.e., temporal) direction, and the "swap" operation makes the head hop horizontally to a vertical line adjacent to the one on which it is currently located. Using these operations, one could deal with much more atoms.

While this seems to have solved the problem of handling a large number of atoms, from the technical point of view the method based on the time discretization is rather different from other worm algorithms on discrete space, requiring programmers to write different programs. In this article, we introduce a simpler approach to continuous systems that is the most natural extension of the worm algorithm and can profit directly from the existing computer codes based upon the discrete space. We simply discretize a continuous system to make it a simple-cubic-lattice system with lattice spacing b as shown in Sec. II, and adopt directed-loop algorithm (DLA) [12,13]. However, straightforward application fails to yield an efficient algorithm as we discuss below, which may be the reason why this approach has not been taken so far. In what follows we show how we solve this problem.

The DLA, which is a hybrid of the loop algorithm and the worm algorithm, has very wide applicability. From world-line configurations we generate graphs in a similar way to the loop algorithm, and then we update world-line configurations by creating a worm and letting it move around in a similar way to the worm algorithm. Unlike the original worm algorithm, however, the head's direction of motion is altered only at vertices that are distributed stochastically before the creation of the worm. Vertices are placed between two vertical lines adjacent to each other, or on a single line. In the former case, a vertex represents a two-body interaction and is visualized as a short horizontal line connecting two vertical lines, whereas in the latter case it represents a one-body interaction and is visualized as a dot placed on a vertical line. In either case, they are distributed stochastically with some density determined by the diagonal matrix element of the Hamiltonian. For a more detailed description, see, for example, Ref. [13]. However, when one applies the method to a system such as the Bose-Hubbard model with $t \ll U$ (t is the hopping amplitude and U is the on-site energy), the efficiency of the straight-forward application of the DLA is low

because of high density of vertices due to large U. In the present paper, we first discuss this difficulty in Sec. III A. Then, we improve the DLA by omitting the vertices generated by the interaction U and taking it into account in other procedures. We also demonstrate the efficiency of the resulting method by applying it to the interacting dilute Bose gas system with a large U.

II. BOSE GAS SYSTEM AND SPACE DISCRETIZATION

In this paper, we focus on dilute Bose gas systems [14]. We here consider the case of three dimensions for concreteness, although the generalization to other cases is straightforward. The Hamiltonian of the interacting Bose gas system in the continuous space is defined as

$$\mathcal{H}_0 = \int d\boldsymbol{r}\left[\frac{\hbar^2}{2m}\boldsymbol{\nabla}\hat{\Psi}^\dagger(\boldsymbol{r})\cdot\boldsymbol{\nabla}\hat{\Psi}(\boldsymbol{r}) - \mu\hat{\Psi}^\dagger(\boldsymbol{r})\hat{\Psi}(\boldsymbol{r})\right] + \frac{1}{2}\int\int d\boldsymbol{r}'d\boldsymbol{r}\hat{\Psi}^\dagger(\boldsymbol{r})\hat{\Psi}^\dagger(\boldsymbol{r}')U(\boldsymbol{r}-\boldsymbol{r}')\hat{\Psi}(\boldsymbol{r}')\hat{\Psi}(\boldsymbol{r}). \tag{1}$$

The operators $\hat{\Psi}$ and $\hat{\Psi}^\dagger$ are field operators of bosons that fulfill the commutation relation $[\hat{\Psi}(\boldsymbol{r}),\hat{\Psi}^\dagger(\boldsymbol{r}')]=\delta(\boldsymbol{r}-\boldsymbol{r}')$, and μ is the chemical potential. We consider only the contribution of s-wave scattering, that is, $U(\boldsymbol{r}-\boldsymbol{r}')=U_0\delta(\boldsymbol{r}-\boldsymbol{r}')$, where U_0 is defined as $U_0=4\pi\hbar^2a/m$, with a being the s-wave scattering length. We assume the repulsive interaction $a>0$.

To simulate the continuous system, we discretize it with a small lattice spacing b. The Hamiltonian is then transformed to the following:

$$\mathcal{H} = t\sum_{\boldsymbol{R}}\sum_{\delta}\{(\hat{\phi}^\dagger_{\boldsymbol{R}+\delta}\hat{\phi}_{\boldsymbol{R}+\delta}+\hat{\phi}^\dagger_{\boldsymbol{R}}\hat{\phi}_{\boldsymbol{R}}) - (\hat{\phi}^\dagger_{\boldsymbol{R}+\delta}\hat{\phi}_{\boldsymbol{R}}+\hat{\phi}^\dagger_{\boldsymbol{R}}\hat{\phi}_{\boldsymbol{R}+\delta})\} - \mu\sum_{\boldsymbol{R}}\hat{\phi}^\dagger_{\boldsymbol{R}}\hat{\phi}_{\boldsymbol{R}} + \frac{u}{2}\sum_{\boldsymbol{R}}\hat{\phi}^\dagger_{\boldsymbol{R}}\hat{\phi}^\dagger_{\boldsymbol{R}}\hat{\phi}_{\boldsymbol{R}}\hat{\phi}_{\boldsymbol{R}}, \tag{2}$$

where $t\equiv\hbar^2/(2mb^2)$ and $u\equiv U_0/b^d$. In this transformation, we have replaced integrals by sums, $\int d\boldsymbol{r}\to b^d\Sigma_{\boldsymbol{R}}$, and Dirac's delta function by Kronecker's delta, $\delta(\boldsymbol{r}-\boldsymbol{r}')\to b^{-d}\delta_{\boldsymbol{R}\boldsymbol{R}'}$. The field operator $\hat{\Psi}^\dagger(\boldsymbol{r})(\hat{\Psi}(\boldsymbol{r}))$ has been replaced by the operator $\hat{\phi}^\dagger_{\boldsymbol{R}}(\hat{\phi}_{\boldsymbol{R}})$, which creates (annihilates) a boson at the site $\boldsymbol{R}$,

$$\hat{\Psi}(\boldsymbol{r})\to b^{-(d/2)}\hat{\phi}^\dagger_{\boldsymbol{R}}. \tag{3}$$

Then, these operators fulfill the commutation relation $[\hat{\phi}_{\boldsymbol{R}},\hat{\phi}^\dagger_{\boldsymbol{R}'}]=\delta_{\boldsymbol{R}\boldsymbol{R}'}$. Note that the on-site interaction u/t becomes larger, as we make the lattice spacing b smaller in order to reduce the discretization error.

Now we have five length scales, three physical and two artificial. The physical length scales are the mean particle distance l, the de Broglie wave length λ_{dB}, and the s-wave scattering length a whereas the artificial two are the lattice spacing b and the system size Λ. In order to make the simulation result accurate, the lattice spacing must be smaller than any one of the three physical length scales, and the system size must be larger than any one of the three; $b\ll l\ll\Lambda$, $b\ll\lambda_{\mathrm{dB}}\ll\Lambda$, and $b\ll a\ll\Lambda$. In what follows, we consider the case where $a\sim l\sim\lambda_{\mathrm{dB}}$. The condition $l\sim\lambda_{\mathrm{dB}}$ is to study the phase transitions of BEC. The other condition $a\sim l$ is to study the effect of the interaction. [The effect of the interaction is recognizable only if the two-body interaction energy is comparable to (or larger than) the kinetic energy. The interaction energy is $E_{\mathrm{int}}\sim\rho U_0$, where $\rho=l^{-3}$, namely, $E_{\mathrm{int}}\propto a/l^3$, whereas the kinetic energy is $E_{\mathrm{kin}}\propto\lambda_{\mathrm{dB}}^{-2}\sim l^{-2}$. Therefore, the kinetic energy and the interaction energy are comparable when $a\sim l$.]

In the DLA, weights of configurations with the worm are determined by adding the source term $\eta_{\mathrm{sim}}\hat{Q}$ to the Hamiltonian. Therefore, we consider the Hamiltonian $\mathcal{H}-\eta_{\mathrm{sim}}\hat{Q}$, where η_{sim} is a tunable parameter. The operator $\hat{Q}$ is the sum of local operators, $\hat{Q}=\Sigma_{\boldsymbol{R}}\int d\tau\{\hat{\phi}^\dagger_{\boldsymbol{R}}(\tau)+\hat{\phi}_{\boldsymbol{R}}(\tau)\}/2$, where τ is imaginary time.

III. METHOD

In this section, we first describe the difficulty that arises from a large on-site interaction. Then, we present a new technique that eliminates this difficulty.

A. The conventional DLA and its problem in the case of fine mesh

In the DLA, the Boltzmann weight of world-line configurations is reflected by the density of vertices. A vertex is defined either on a single space-time point (one-site vertex) or on a pair of points that have the same temporal coordinate and different spatial ones (two-site vertex). While the one-site vertices represent one-body interactions such as the U term in the Hubbard model, the two-site vertices correspond to two-body interactions such as the kinetic energy term. Two-site vertices are placed between two vertical lines with the density $\rho_{ij}[\psi_{ij}]=\langle\psi_{ij}|-\mathcal{H}_{ij}|\psi_{ij}\rangle$ when the Hamiltonian is the sum of local terms, i.e., $\mathcal{H}=\Sigma_{(i,j)}\mathcal{H}_{ij}$. The indices i and j specify spatial positions (namely, sites) and $\rho_{ij}[\psi_{ij}]$ is the density of vertices that connects the sites i and j. The symbol ψ_{ij} stands for the state of these two sites at the imaginary time at which the vertices are to be placed. All the diagonal elements of the Hamiltonian need to be negative because the density must be positive. We therefore introduce some constant real number E_U, and replace the original Hamiltonian by $\mathcal{H}'=\mathcal{H}-E_U$, whose diagonal elements are all negative. In what follows, we denote the new Hamiltonian simply as $\mathcal{H}$.

In the region $t\leqslant u$, namely, $\hbar^2b/m\leqslant U_0$, the constant E_U should be chosen such that $E_U>n_{\max}^2U_0/(2b^3)$, where $n_{\max}$ is the cutoff of the occupation number, which we fix in advance. In dilute gases, the most probable state is the one in which both the site i and j are vacant. In this state, the vertices are placed with density $\rho_{ij}>n_{\max}^2U_0/(2b^3)$, which diverges as $b\to0$. Although in most cases a worm head simply passes the vertex without changing the direction, this passage consumes a finite amount of CPU time, and as $b\to0$ this process becomes the most time consuming part of the whole computation. Therefore, it would be highly desirable to find

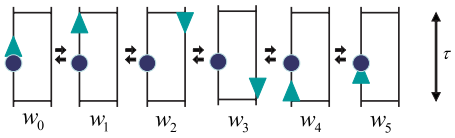

FIG. 1. (Color online) One example of the path that the worm updates the configuration: the triangle and the circle, respectively, show the head and the tail.

a way to avoid such a waste of computer resources. The modification of DLA described in the next subsection keeps the number of the vertices from diverging when the mesh becomes finer.

B. Modification of directed-loop algorithm

We here propose a method in which only the two-site interaction term is reflected in the density of the vertices and the one-site term (i.e., the U term) is treated separately. For this purpose, we define the Hamiltonian (2) as the sum of the U term and the rest: $\mathcal{H}=\mathcal{H}^t+\mathcal{H}^U$, where $\mathcal{H}^U$ is $\mathcal{H}^U=(u/2)\Sigma_{\boldsymbol{R}}\hat{\phi}^\dagger_{\boldsymbol{R}}\hat{\phi}^\dagger_{\boldsymbol{R}}\hat{\phi}_{\boldsymbol{R}}\hat{\phi}_{\boldsymbol{R}}$. An update cycle of the new method includes assignment of two-site vertices and placement of the worm, with the densities and the probabilities obtained by the conventional DLA prescription applied to $\mathcal{H}^t$. The new ingredient, which takes care of $\mathcal{H}^U$, is the stochastic determination of passage of a segment delimited by the two vertices. In other words, in contrast to the conventional DLA, the head may not reach the next vertex (i.e., the other end of the segment that lies ahead of it). As a result, in addition to the scattering probability for determining the outgoing direction of the head after scattered by the two-site vertex, we need to introduce a segment-passage probability with which we allow the head to reach the next vertex. The segment-passage probability reflects $\mathcal{H}^U$ as described below.

We start from the Suzuki-Trotter decomposition of the Boltzmann factor. Assuming that $\mathcal{H}^t$ is expressed as $\mathcal{H}^t=\Sigma_{b=1}^M\mathcal{H}^t_b$ with b specifying a pair of nearest neighbor sites, the partition function can be expressed as

$$Z=\lim_{L\to\infty}\sum_{\{\psi\}}\prod_{k=1}^{L}\prod_{b=1}^{M}\times\left\langle\psi_b(k+1)\left|\sum_{G=0,1}(-\Delta\tau\mathcal{H}^t_b)^G\right|\psi_b(k)\right\rangle\times\prod_{i=1}^{N}\langle\psi_b(k)|e^{-\Delta\tau\mathcal{H}^U_i}|\psi_b(k)\rangle, \quad (4)$$

where $\Delta\tau=\beta/L$. Based on this expression, let us consider the hypothetical process depicted in Fig. 1 by which the worm's head transforms a state into another. By examining the change in the weight of the corresponding intermediate state, we may obtain the proper segment-passage probability.

In Fig. 1, w_α denotes the total weight of the state $\alpha=0,1,\ldots,5$. Note that vertical moves of the head change the total weight because of the U term. Denoting the probability of the transition from the state β to the state α as $t_{\alpha\beta}$, the detailed-balance condition to be fulfilled by this hypothetical process is

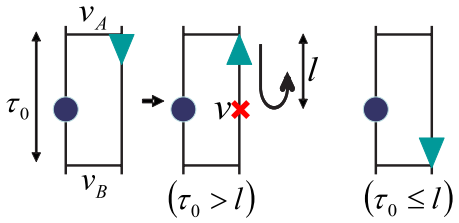

FIG. 2. (Color online) An imaginary process where the head turns back at and passes through one-site vertex.

$$t_{54}t_{43}t_{32}t_{21}t_{10}w_0=t_{01}t_{12}t_{23}t_{34}t_{45}w_5. \quad (5)$$

The probabilities of scattering at the vertices (i.e., t_{12}, t_{34}, t_{43}, t_{21}) are determined by the conventional DLA prescription for $\mathcal{H}_t$. The probabilities of the head's vertical move (i.e., t_{01}, t_{23}, t_{45}, t_{54}, t_{32}, t_{10}) are obtained from the Metropolis method, i.e.,

$$t_{ij}=\frac{\min(w_i,w_j)}{w_j}, \quad (6)$$

which automatically satisfy Eq. (5). For the present model, for example, the probability of a head passing a segment whose length is τ and occupation number is n is $t_+=e^{-un\tau}$ if the head increases the local occupation number. On the other hand, if it decreases the occupation number, the passage probability is always 1, i.e., $t_-=1$.

Obviously no single-site vertex is placed in the new method. Therefore, this method solves the problem of too many one-site vertices that would be generated if we applied the conventional DLA prescription to the whole Hamiltonian in a straight-forward fashion. In fact, the procedure described above could be obtained by "renormalizing" the single-site vertices as we discuss in the next subsection and also in Appendix A. In the straightforward DLA (applied to the whole Hamiltonian), vertices are placed with the density $\rho\sim un^2_{\max}$. In contrast, in the modified DLA, the density of two-site vertices is $\rho\sim tn_{\max}$. The total CPU time is proportional to the density of vertices, because the most time-consuming part of the code is spent on the head's passing (or scattering) at vertices. Therefore, the CPU time for the straightforward DLA is roughly $\mathcal{O}(an_{\max}/b)$ times larger than that for the modified DLA.

C. Measured quantities

In a simulation with the conventional DLA, we measure the two-point correlation function as the frequency of worm's head visiting a particular position. As a result, the susceptibility is reduced to the average length of the path of the head. However, because of the modification we make, this simple relation must be modified as we see below.

Let us first consider the conventional DLA with one-site vertices and an event where the head is bounced at some two-site vertex v_A, as shown in Fig. 2. We interpret this event as that the head first passes the vertex v_A, proceed for a distance l, and turns back at a one-site vertex v that is located there. Let the length of the segment along which the head travels be τ_0, and consider a uniform random number $R\in[0,1)$. Then, the distance l is determined as

$$l = \tau_0 \frac{\ln(1-R)}{\ln t}. \tag{7}$$

(If $l > \tau_0$, we let the head proceed to the next vertex v_B without bouncing.) Equation (7) is consistent with the result of the conventional DLA which explicitly deals with the one-site vertices. For the derivation of Eq. (7), see Appendix A.

In the present paper, we focus on two physical quantities, two-point correlation function in the real space $C(\boldsymbol{R},\boldsymbol{R}')$ defined as

$$C(\boldsymbol{R},\boldsymbol{R}') \equiv \langle \hat{\phi}^{\dagger}_{\boldsymbol{R}} \hat{\phi}_{\boldsymbol{R}'} \rangle, \tag{8}$$

and susceptibility χ defined as

$$\chi = \int_0^{\beta} d\tau \sum_{\boldsymbol{R}} \langle \hat{\phi}^{\dagger}_0(\tau) \hat{\phi}_{\boldsymbol{R}}(0) \rangle, \tag{9}$$

where τ means the imaginary time and β the inverse temperature. If the system under consideration is homogeneous, $C(\boldsymbol{R},\boldsymbol{R}')$ depends only on relative position $\boldsymbol{R}-\boldsymbol{R}'$. We consider an event that the head visits a point of which the space-time coordinate is $(\boldsymbol{R},0)$. (Here, the origin of the coordinate is the position of the worm's tail.) We define $n_{\mathrm{visit}}(\boldsymbol{R})$ as the number of occurrence of such events in a cycle (i.e., from a worm's creation to its annihilation). We also define l_w as the average traveling length of the head per cycle. It is necessary to count hypothetical processes as shown in Fig. 2 when we measure n_{visit} and l_w. In other words, when the head turns back at a vertex v_A in the modified DLA algorithm, we should regard it as that the head actually passes v_A once, reach an imaginary one-site vertex v, turns around there, and comes back to v_A, as shown in Fig. 2. With this interpretation, the quantities $C(\boldsymbol{R})$ and χ can be obtained from $n_{\mathrm{visit}}(\boldsymbol{R})$ and l_w as

$$C(\boldsymbol{R}) = \left(n_{\max} - \frac{1}{2}\right) n_{\mathrm{visit}}(\boldsymbol{R}), \tag{10a}$$

$$\chi = \left(n_{\max} - \frac{1}{2}\right) l_{\mathrm{w}}. \tag{10b}$$

IV. SIMULATION

A. Technical parameters

In the simulations discussed below, we set the upper bound on the occupation number as $n \leqslant n_{\max}=5$, which ensures that $\rho \ll n_{\max} b^{-3}$ with ρ being the density of particles. We also choose $\eta_{\mathrm{sim}} = \sqrt{2/\{V\beta(2n_{\max}-1)\}}$, where V is the volume of the system and β the inverse temperature. This is the largest possible choice of all feasible values. If η_{sim} is larger than this value, the probability of generation of a worm in some cases becomes negative. For each set of simulation, we start from the vacuum state with no particles. The first n_{dump} sweeps are just for equilibrating the system, and not counted. Then, successive n_{MCS} sweeps are counted for the measurement. We use $n_{\mathrm{dump}} \sim 2500$ and $n_{\mathrm{MCS}} \sim 10\,000$.

Since we simulate the grand canonical ensemble, the number of particles fluctuates freely. However, in the case of the ideal Bose gas system discussed in the next subsection, varying temperature with fixed average occupation ρ, instead of fixed chemical potential μ, is more convenient because we cannot observe a phase transition at a finite μ in the thermodynamic limit. Therefore, we have adjusted the chemical potential μ at each temperature so as to make the average density ρ takes some constant value fixed in advance. In order to choose the right value of μ, we have employed the steepest descent method. In the case of the interacting Bose gas system, on the other hand, we investigated the temperature dependence of various quantities with fixed μ.

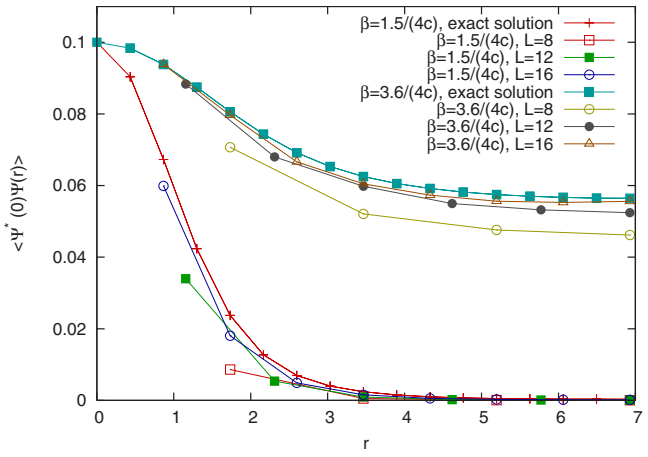

FIG. 3. (Color online) The two-point Green's function of the ideal Bose gas at $\beta=1.5/(4c)$, $3.6/(4c)$, and $n_{\max}=5$. $L=\Lambda/b$. [$n_{\max}$ may not be large enough in the case $L=8$, $\beta=3.6/(4c)$ and this may introduce small errors to the data.]

B. Space-discretization of ideal Bose gas system

In order to demonstrate the efficiency of the algorithm, we first consider the ideal Bose gas system because it is a convenient test case for which the exact solution is available. In this case, the algorithm reduces to a conventional DLA.

For a cubic system whose liner size is Λ, the correlation function is

$$C(\boldsymbol{r},\Lambda) = \frac{1}{\Lambda^3} \sum_{\boldsymbol{k}} \frac{\cos \boldsymbol{k}\cdot\boldsymbol{r}}{e^{\beta(ck^2-\mu)}-1}, \tag{11}$$

where $c=\hbar^2/(2m)$ and the summation is taken for $\boldsymbol{k}=(2\pi/\Lambda)(n_x,n_y,n_z)$, with n_x, n_y, and n_z being integers ranging from 0 to ∞. The convergence in the continuum limit can be clearly seen in Fig. 3 that shows the correlation function $C(\boldsymbol{r},\Lambda=8)$ for various coarseness of space discretization. The correlation is measured along the diagonal direction, i.e., $\boldsymbol{r}=(r,r,r)$. In all the simulations presented in Fig. 3, the chemical potentials μ is adjusted to make the particle density approximately 0.1.

We next see the finite-size scaling properties of the susceptibility χ. Figure 4 shows the finite size scaling of χ. More specifically, we assume the form $\chi=\Lambda^{2-\eta}\tilde{\chi}(t\Lambda^{1/\nu})$. The calculation has been done with density $\rho=0.1$, and the lattice spacing $b=1/2$. The values of the critical exponents used for the fitting are $\eta=0$ and $\nu=1$, the exact values for the ideal

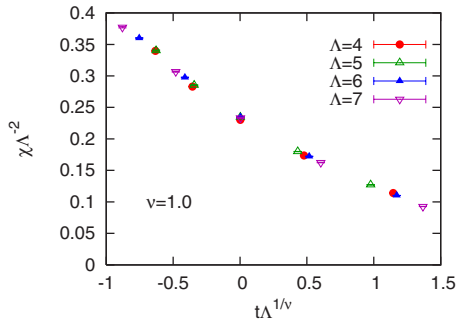

FIG. 4. (Color online) Finite size scaling of the integrated Green's function with $\beta_c=2.802$, $b=1/2$.

gas (see Appendix B). A relative temperature t is defined as $t \equiv T-T_c$. For T_c, we use the value for the continuous system. In principle, the exact critical temperature of the discrete system differs from that of the continuous system. Nevertheless, the finite size scaling with T_c for the continuous system works well, which implies that the lattice spacing b is sufficiency small. (See Appendix C for more details of the convergence of physical quantities in the limit of $b \to 0$.)

C. Modified directed-loop algorithm for Bose gas system with interaction

Having seen how the present method works for the noninteracting model, we next demonstrate the validity of the method in a more nontrivial case. We take the hopping energy t as our unit of energy and the double of the lattice spacing $2b$ as our unit of distance below. We fix the chemical potential as $\mu=0.5$, and choose the values of the interaction energy as $u=96.0$ ($a \simeq 1.91$). From the finite size scaling of χ, as we see below, we estimate the critical temperature as $T_c=0.76\pm0.01$. The average particle distance l is measured as $l=1.414(2)$, where the system size is $\Lambda=8$, and the inverse temperature is $\beta=1.3$. Therefore, our choice of physical parameters fulfills the requirement for a reasonable approximation (i.e., $b<a<\Lambda$ and $b<l<\Lambda$).

Because of the symmetry of the Hamiltonian (2), the critical phenomena of this system should belong to the universality class of the XY model in three dimensions. According to a recent work [15], critical exponents of the XY model in three dimensions are

$$\nu = 0.6723(3), \tag{12a}$$

$$\eta = 0.0381(2). \tag{12b}$$

Figure 5(a) shows the finite size scaling of χ using these values of the exponents. On the other hand, the values of the ideal Bose gas are used in Fig. 5(b) for the same set of the data for comparison. At a first glance, the ideal gas exponents seem to fit the data better than the ones for the three-dimensional XY model. However, we can see that this is not so when we take a closer look at the critical region. In Fig. 5(a′) and Fig. 5(b′) are the enlarged views of Fig. 5(a) and Fig. 5(b), respectively. Whereas agreement of the curves with different system sizes becomes better as one approaches the critical point in (a) and (a′), we can observe a clear systematic deviation from a single curve in (b) and (b′).

The apparent better agreement for the ideal gas universality class in Figs. 5(a) and 5(b) is the result of the crossover from the noninteracting regime to the interacting regime. Since we have studied the case of a weak interaction, this crossover makes the asymptotic scaling region rather narrow in temperature. In order not to be deceived by the apparent behavior and to identify the correct universality class, we need a very accurate numerical simulation and a careful analysis. The present case demonstrates that the new method is indeed efficient enough to distinguish between universality

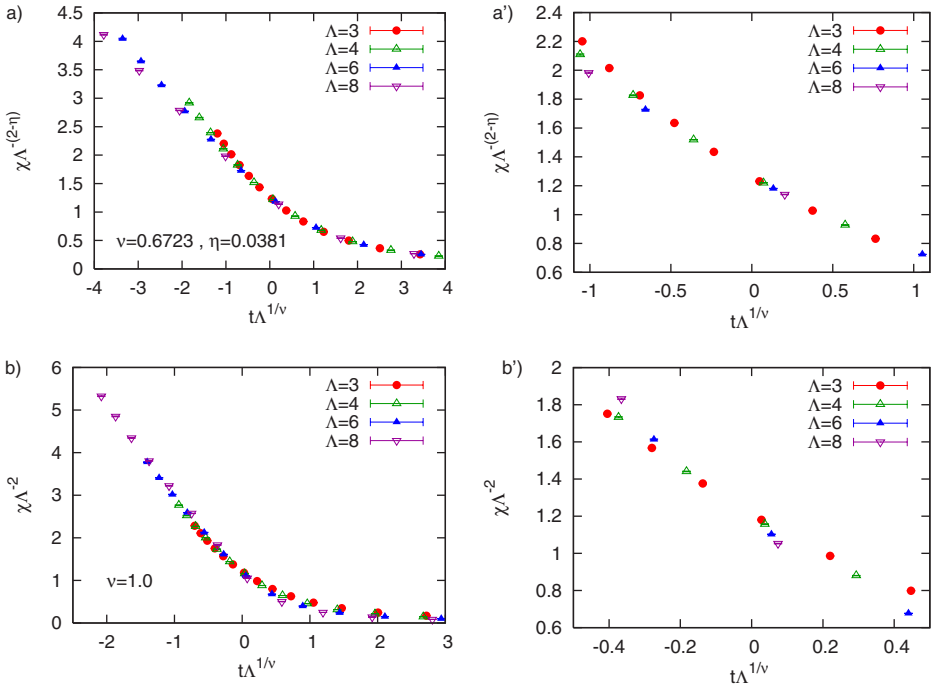

FIG. 5. (Color online) Finite-size-scaling plots of the integrated one-body Green's function: (a) with the exponents of XY model and with $T_c=0.76\pm0.01$, (a′) the enlarged view of (a), (b) with the exponents of the ideal Bose gas and with $T_c=0.76$, and (b′) the enlarged view of (b). The symbol t stands for $T-T_c$.

TABLE I. Comparison between the modified DLA and the conventional DLA. The system size is $\Lambda=6\times(2b)$, The parameters are chosen as follows: the chemical potential as $\mu=0.01t$, the inverse temperature as $\beta t=3.0$, the s-wave scattering length as $a=2.0\times(2b)$, the maximum occupation number as $n_{\max}=5$, the number of sweeps for sampling as $n_{\mathrm{MCS}}=51\,200$, and the number of sweeps for equilibration as $n_{\mathrm{dump}}=2500$.

	Conventional	Modified
CPU time (s)	8.7×10^5	2.4×10^4
Maximum number of vertices	6.5×10^5	4.8×10^4
Average number of vertices	6.4×10^5	2.3×10^4
Estimated average occupation number	0.011 23(3)	0.011 19(4)

classes and discuss the correct scaling properties.

V. DISCUSSION

In this section, we first take a closer look at the efficiency of the new method and compare it with the conventional DLA. Table I shows the CPU time spent for the simulation on a single processor of SGI Altix 3700 for two methods. In both cases, the same number of Monte Carlo sweeps have been carried out. The resulting accuracy of various quantities are roughly the same. As an example, the estimated average occupation number together with its estimated statistical error are presented in Table I. As is also clear from the table, the calculation with the modified DLA has been executed about 36 times faster and the memory usage has been reduced by the factor of 93%.

In this article, we have studied the space-discretized Bose gas systems Eq. (2). We have demonstrated the validity of the space-discretization approach to the continuous limit by simulating the noninteracting and interacting Bose gas system. For the interacting system with the repulsive interaction, we have argued that the straightforward application of the conventional DLA is not practical since the relative magnitude of the interaction in the discretized model u/t always becomes large as we make the lattice spacing smaller $b\to0$ in order to reduce the systematic error due to the discretization. We have therefore modified the DLA to solve the problem. By this modification we eliminate all the single-site vertices that would result from the interaction u, improving the efficiency of simulations dramatically. Finally, we have demonstrated that the new scheme, i.e., the space discretization with the modified DLA, is a promising approach to the phase transitions in the interacting Boson systems by presenting some results of the simulations using the new method.

ACKNOWLEDGMENTS

The simulations are carried out at the Supercomputer Center, Institute for Solid State Physics, University of Tokyo. The present work is financially supported by MEXT Grant-in-Aid for Scientific Research (B) 19340109 (2007) and by Next Generation Supercomputing Project, Nanoscience Program, MEXT, Japan.

APPENDIX A: MEASUREMENT OF THE WORM LENGTH

After being scattered at a two-site vertex, say v_1, the head travels along a segment that is delimited by v_1 and another vertex, say v_2. In the straightforward application of the DLA, in general, there are many one-site vertices on this segment. The head may or may not be scattered at one of these one-site vertices. If it is scattered once, it comes back to v_1, whereas if it is not scattered at any one-site vertex, it goes through the segment and reaches v_2. As we have seen in Sec. III B, we can compute the probability of the head returning to v_1 or going through to v_2 without performing passing/scattering events at one-site vertices. Therefore, we do not have to deal with one-site vertices in real computation. Here, we use the original picture again, in order to obtain formulas for computing two-point correlation functions and the susceptibility. Once we obtain the formulas, we can compute these quantities in real computation without scattering at one-site vertices.

We first decompose the Hamiltonian as $\mathcal{H}=\mathcal{H}^t+\mathcal{H}^U$. The term $\mathcal{H}^U$ can be expressed as $\mathcal{H}^U=\Sigma_i U(n_i)$ where $U(n_i)\equiv(u/2)n_i(n_i-1)$. Then, vertices arising from $\mathcal{H}^U$, namely one-site vertices, can be expressed as dots on a vertical line. For a vertical line that corresponds to the site i, the vertices should be placed on it with imaginary-time dependent density $W_k=U(n_i(\tau))$, where $n_i(\tau)$ is the occupation number on the site i and at the imaginary time of τ. In real computation, this vertex placement is achieved by two steps as follows. First, we stochastically generate n_v, the total number of vertices to be placed on a segment, according to Poisson distribution

$$P_{n_v}(\Delta\tau\rho)=\frac{(\Delta\tau\rho)^{n_v}}{n_v!}e^{-\Delta\tau\rho}, \tag{A1}$$

where $\Delta\tau$ is the length of the segment. Then, we place n_v vertices on the segment simply by generating n_v independent uniform random numbers in the interval $[0,\Delta\tau)$.

Next, we consider the probability of the head passing/bouncing at a single-site vertex. This is formally written as $t_{\alpha\beta}$, the transition probability to a state α from a state β. Denoting the weight of the state β as w_β, we write the transition probability as $t_{\alpha\beta}=w_{\alpha\beta}/w_\beta$. Then, $w_{\alpha\beta}$ must satisfy two conditions $w_{\alpha\beta}=w_{\beta\alpha}$, and $w_\beta=\Sigma_\gamma w_{\gamma\beta}$. Figure 6 shows an example of $w_{\alpha\beta}$ satisfying these conditions. A cross denotes a single-site vertex, and a triangle the head in Fig. 6. For the scattering at the single-site vertex, we have to consider the vertex weight W_k only since other factors would not be changed by the scattering. In Fig. 6, we assume $n_{\max}=2$ and $w_{32}=0$ for the sake of simplicity.

Figure 7 schematically shows a possible motion of the worm's head along a vertical segment whose length is $\Delta\tau$. Changing the local state behind it from k to $k+1$, the head passes all the single-site vertices until it finally arrives at a vertex in the imaginary time interval (τ_0+l,τ_0+l+dl) where τ_0 is the imaginary time of the last visited two-site vertex. We here assume that $W_{k+1}\leqslant W_k$. Then, the probability of this process being chosen is a product of three probabilities:

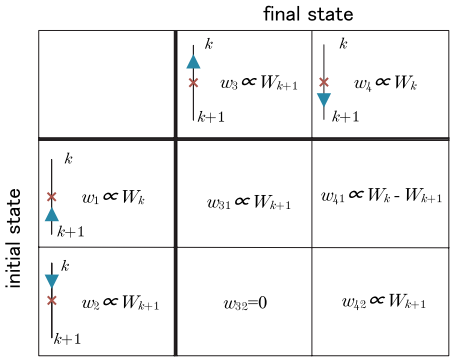

FIG. 6. (Color online). The weight $w_{\alpha\beta}$. A triangle and a cross represent the head of the worm and a single-site vertex, respectively.

$$P(l)dl = \left[\sum_{n_v=0}^{\infty} P_{n_v}(lW_k)\left(\frac{W_{k+1}}{W_k}\right)^{n_v}\right] \times [W_k dl] \times \left[1 - \frac{W_{k+1}}{W_k}\right]. \tag{A2}$$

The first factor is the probability of the head traveling the distance l without being scattered by any vertex. The second is the probability of finding a vertex in the interval $l \sim l+dl$. The third is the probability that the head is bounced back there. Thus we obtain the density

$$P(l) = (W_k - W_{k+1})e^{-(W_k - W_{k+1})l}. \tag{A3}$$

In order to take into account the contributions from the imaginary round trip between the two-site vertex and the one-site vertex, we have only to generate a random number l according to the distribution $P(l)$ and add $2l$ to the traveling length every time the head fails to pass a segment. In fact, the decision of passing or bounce and, in the case of bounce, the calculation of the length of the imaginary roundtrip can be done at the same time as follows. Every time the head leaves a two-site vertex, we generate l according to $P(l)$, i.e., generate a uniform random number R and define

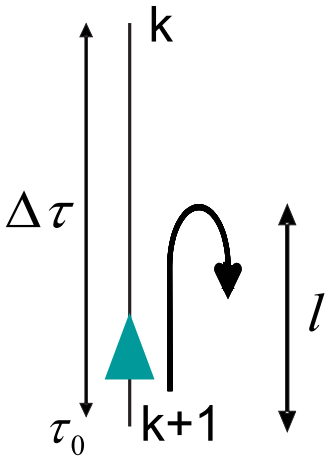

FIG. 7. (Color online). The motion of the head which turns back at $\tau_0 + l$.

$$l \equiv \frac{|\ln R|}{W_k - W_{k+1}}. \tag{A4}$$

If $l > \Delta\tau$, where $\Delta\tau$ is the length of the segment that lies ahead of the head, we let the head move to the next two-site vertex and add $\Delta\tau$ to the working sum of the traveling length. If not, we let the head turn around and add $2l$ to the sum.

APPENDIX B: THE SCALING LAW OF THE IDEAL BOSE GAS

In this section, we derive the critical exponents ν and η of the ideal Bose gas. The exponents are defined as $\xi \propto t^{-\nu}$, and $C(r)_{\beta=\beta_c} \propto 1/r^{d-2+\eta}$, where ξ is correlation length, t is relative temperature $T - T_c$, and $C(r)$ is the correlation function defined as

$$C(|\boldsymbol{r}|) \equiv \langle \hat{\Psi}^\dagger(\boldsymbol{0})\hat{\Psi}(\boldsymbol{r})\rangle. \tag{B1}$$

The particle density of the ideal Bose gas near the criticality is given by

$$\rho \sim T^{3/2}\left(A - B\sqrt{-\frac{\mu}{T}}\right), \tag{B2}$$

where A and B are the coefficients in the expansion of the Appell function [16]

$$F(y) \equiv \int_0^\infty dx \frac{\sqrt{x}}{e^{x+y} - 1} \approx A - B\sqrt{y}. \tag{B3}$$

Therefore, with fixed density we obtain the temperature dependence of μ as

$$\mu \approx -\frac{3A}{2BT_c}t^2. \tag{B4}$$

We can express the correlation function of the infinite continuous system $C(r)$ as

$$C(r) = \rho_0 + \frac{1}{(2\pi)^3}\sum_{l=1}^{\infty}\left(\sqrt{\frac{\pi}{lc\beta}}\right)^3 \exp\left(l\beta\mu - \frac{r^2}{4lc\beta}\right), \tag{B5}$$

where ρ_0 is density of condensate and $c = \hbar^2/(2m)$. Note that the exponent in the summand has a peak at $l = l^* = r/\{2\beta\sqrt{(-\mu)}\}$. We therefore expand it around l^*. Up to the second order in $x \equiv l - l^*$, we obtain

$$l\beta\mu - \frac{r^2}{4lc\beta} \simeq 2l^*\beta\mu + \frac{\beta\mu}{l^*}x^2. \tag{B6}$$

Then, the second term of Eq. (B5) is reduced to

$$\frac{1}{(2\pi)^3}\sum_{l=1}^{\infty}\left(\sqrt{\frac{\pi}{lc\beta}}\right)^3 \exp\left(l\beta\mu - \frac{r^2}{4lc\beta}\right) \simeq \frac{1}{(2\pi)^3}\int_{-\infty}^{\infty} dx\left(\sqrt{\frac{\pi}{l^*c\beta}}\right)^3 \exp\left(2l^*\beta\mu + \frac{\beta\mu}{l^*}x^2\right),$$

$$= \frac{\sqrt{c}}{4\pi\beta r} \exp\left\{ - \frac{r}{\sqrt{c/(-\mu)}} \right\}, \tag{B7}$$

which yields $\xi = \sqrt{c/(-\mu)}$. Using the t dependence of μ [Eq. (B4)], we find

$$\nu = 1. \tag{B8}$$

In addition, because the chemical potential is $\mu = 0$ at $T = T_c$, it is found that the correlation function is $C(r)_{\beta=\beta_c} \propto 1/r$, which means

$$\eta = 0. \tag{B9}$$

APPENDIX C: CONVERGENCE OF PHYSICAL QUANTITIES

For the ideal Bose gas, by exploiting the exact solution, we can clarify how the density of particle ρ of a discrete system converges to the continuous limit. For $kb \ll 1$, the dispersion relation is

$$\epsilon_{\boldsymbol{k}}(b) \simeq ck^2 - A_{\boldsymbol{k}} b^2 - \mu, \tag{C1}$$

where $A_{\boldsymbol{k}} = c(k_x^4 + k_y^4 + k_z^4)/12$ whereas this term is absent in the case of the continuous system.

We consider the deviation of density $\Delta\rho \equiv \rho(b,\mu) - \rho(0,\mu)$ where $\rho(b,\mu)$ denotes the density at the lattice spacing b and the chemical potential μ. Then, $\Delta\rho$ is approximated as

$$\Delta\rho \simeq \frac{1}{V}\left[\sum_{\boldsymbol{k}} \left(\frac{1}{e^{\beta(ck^2 - A_{\boldsymbol{k}} b^2 - \mu)} - 1} - \frac{1}{e^{\beta(ck^2-\mu)} - 1} \right) + \sum_{k \geq b^{-1}} \frac{1}{e^{\beta(ck^2-\mu)} - 1} \right],$$

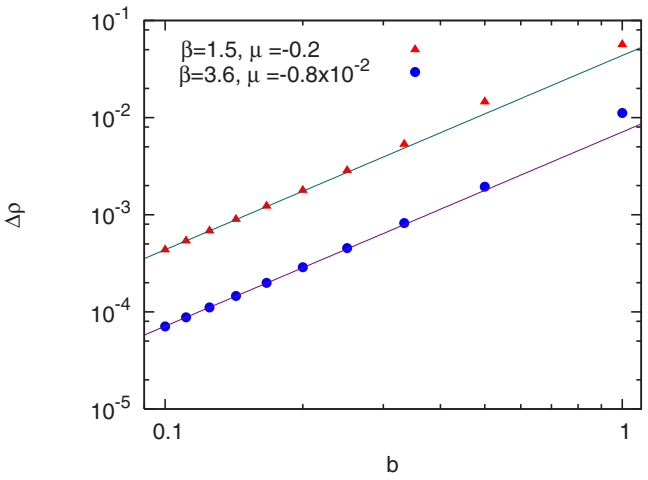

FIG. 8. (Color online). The deviation of the density $\Delta\rho$ vs the lattice spacing b for two sets of parameters $(\beta,\mu) = (1.5,-0.2)$ and $(3.6,-0.08)$. Straight lines represent $0.00712 \times b^2$ and $0.04365 \times b^2$. The resulting particle density of the continuous system is roughly 0.1 for both sets of parameters.

$$\simeq \frac{1}{V} \sum_{\boldsymbol{k}} \frac{e^{\beta(ck^2-\mu)} \beta A_{\boldsymbol{k}} b^2}{\{e^{\beta(ck^2-\mu)} - 1\}^2} \propto b^2. \tag{C2}$$

In deriving the second line, we have ignored the last term in the first line because it decays exponentially as $b \to 0$ and becomes negligible, assuming that b is smaller than the de Broglie wavelength λ_{dB}.

Figure 8 shows $\Delta\rho$. Here we take $\Lambda/8$ as the unit of length and $4c$ as the unit of energy. We compute exact solutions for the lattice system of varying lattice spacing b at two temperatures $\beta = 1.5, 3.6$ using the exact dispersion relation for the cubic lattice. We choose $\mu = -0.2$ at $\beta = 1.5$ and $\mu = -0.8 \times 10^{-2}$ at $\beta = 3.6$. Correspondingly, the de Broglie wavelength is $\lambda_{\mathrm{dB}} \simeq 2.171$ at $\beta = 1.5$ and $\lambda_{\mathrm{dB}} \simeq 3.363$ at $\beta = 3.6$. Solid straight lines, representing $\Delta\rho \propto b^2$, are drawn for comparison. The agreement between these lines and computation results is satisfactory in both cases, confirming the validity of the b dependence derived above.

[1] M. H. Anderson, J. R. Ensher, M. R. Matthews, C. E. Wieman, and E. A. Cornell, Science **269**, 198 (1995).
[2] M. Greiner, O. Mandel, T. Esslinger, T. W. Hansch, and I. Bloch, Nature (London) **415**, 39 (2002).
[3] E. Kim and M. H. W. Chan, Nature (London) **427**, 225 (2004).
[4] S. Wessel and M. Troyer, Phys. Rev. Lett. **95**, 127205 (2005).
[5] D. Heidarian and K. Damle, Phys. Rev. Lett. **95**, 127206 (2005).
[6] R. G. Melko, A. Paramekanti, A. A. Burkov, A. Vishwanath, D. N. Sheng, and L. Balents, Phys. Rev. Lett. **95**, 127207 (2005).
[7] M. Boninsegni and N. Prokof'ev, Phys. Rev. Lett. **95**, 237204 (2005).
[8] M. Boninsegni, N. V. Prokof'ev, and B. V. Svistunov, Phys. Rev. E **74**, 036701 (2006).
[9] D. M. Ceperley, Rev. Mod. Phys. **67**, 279 (1995).
[10] E. L. Pollock and D. M. Ceperley, Phys. Rev. B **36**, 8343 (1987).
[11] M. Boninsegni, Nikolay Prokof'ev, and B. Svistunov, Phys. Rev. Lett. **96**, 070601 (2006).
[12] O. F. Syljuåsen and A. W. Sandvik, Phys. Rev. E **66**, 046701 (2002).
[13] N. Kawashima and K. Harada, J. Phys. Soc. Jpn. **73**, 1379 (2004).
[14] F. Dalfovo, S. Giorgini, L. P. Pitaevskii, and S. Stringari, Rev. Mod. Phys. **71**, 463 (1999).
[15] M. Hasenbusch and T. Török, J. Phys. A **32**, 6361 (1999).
[16] J. E. Robinson, Phys. Rev. **83**, 678 (1951).